A Microstructurally Based Model for Recrystallization in Dual-Phase Steels

ALEXANDRE MATHEVON, VÉRONIQUE MASSARDIER, DAMIEN FABRÈGUE, PHILIPPE ROCABOIS, and MICHEL PEREZ

Adjusting and predicting the ferrite recrystallization kinetics of cold-rolled Advanced High-Strength Steels during annealing is necessary to control their final microstructure and thus their mechanical properties. This study proposes a microstructurally based model for predicting the recrystallization kinetics of Dual-Phase steels that takes into account the effect of several physical parameters (chemical composition, temperature, cold rolling reduction ratio, and precipitation state). First, ternary Fe-C-Mn grades were used to validate the parameters of the model relative to the Mn content and to the reduction ratio. Second, the effect of other alloying elements (Si, Cr, Mo) was analyzed using recrystallization kinetics from the literature, before testing the model on two industrial Dual-Phase grades: a DP600 steel and a micro-alloyed DP1000 steel. The effect of the micro-alloyed elements (Nb,Ti) either in solid solution or as precipitates was detailed. Lastly, the model was used to build interaction maps between recrystallization and austenite formation during continuous heating with different heating rates.

https://doi.org/10.1007/s11661-020-05852-8
© The Minerals, Metals & Materials Society and ASM International 2020

I. INTRODUCTION

DUAL-PHASE (DP) steels are commonly manufactured in the form of thin steel sheets mostly for the automotive industry. They are characterized by a two-phase microstructure mixing a hard martensitic phase (α') embedded in a soft ferritic matrix. This typical ferrite-martensite microstructure is generally produced from a cold-rolled state. The steel sheet is first heated to its annealing temperature T often chosen in the inter-critical domain ($Ac_1 < T < Ac_3$). It is then annealed for a given time t at temperature T leading to a partial austenitization. Lastly, the steel is rapidly quenched to obtain the austenite-to-martensite transformation and the final ferrite-martensite microstructure.

In a recent paper,[1] it was shown that an interaction may occur between recrystallization and austenite formation during the annealing of a micro-alloyed DP1000 steel and that this interaction may have a strong impact on the austenite formation kinetics and subsequently on the mechanical properties. In particular, the paper highlighted that the austenite formation kinetics was all the more accelerated as the fraction of deformed ferrite grains at the beginning of austenite formation was high.

In order to predict the experimental conditions leading to this type of interaction, it is thus absolutely necessary to be able to model the recrystallization kinetics of the Dual-Phase steels which depend on several parameters: (i) the amount of substitutional elements in solution, (ii) the precipitates formed before or during recrystallization, (iii) the reduction ratio, and (iv) the type of thermal cycles (heating rate, annealing temperature, and time).

At present, the modeling of recrystallization in DP steels is not yet fully understood. Three types of approaches can be distinguished in the ongoing studies: (1) full field (*i.e.*, mesh-based like phase field[2] and level set[3–5]), (2) mean field (*i.e.*, statistical, but usually physically based like cellular automaton[6,7] and Monte-Carlo), and (3) phenomenological (*e.g.*, JMAK model).

Full field methods account for complex 3-D simulations based on real or simulated microstructures. However, they generate very long computational times and cannot be easily extended to different steel compositions due to the number of assumptions and input parameters.

The Johnson–Mehl–Avrami–Kolmogorov (JMAK) approach describes the evolution of the transformed fraction F(T,t) (with $0 < F(T,t) < 1$) as a function of

ALEXANDRE MATHEVON, VÉRONIQUE MASSARDIER, DAMIEN FABRÉGUE and MICHEL PEREZ are with the Univ. Lyon - INSA Lyon - MATEIS - UMR CNRS 5510, Bât. Saint-Exupéry, 25 Avenue J. Capelle, 69621, Villeurbanne Cedex, France. Contact e-mail: veronique.massardier@insa-lyon.fr PHILIPPE ROCABOIS is with the Fives Keods, 102 Avenue de la Liberté, Maisons-Alfort, France.

Manuscript submitted January 30, 2020.

Published online: 14 June 2020

Table I. Values of the JMAK Parameters Determined on Different Steels in the Literature

Authors	Grades	Reduction Ratio	n	b_0 (s^{-1})	Q (kJ/mol)
Kulakov[8]	0.1C-1.8Mn-0.15Si-0.35Cr (DP600)	50 pct	1.7	1.1×10^{17}	342
Li [9]	0.1C-1.6Mn-0.4Si (DP590)	70 pct	1.45	5.5×10^{19}	384
Yang[10]	0.08C-1.5Mn-0.2Si	25 to 50 pct	—	—	226 to 272
Huang[11]	0.18C-1.55Mn-1.7Si (TRIP)	55 pct	1	1.6×10^{18}	350
Huang[11]	0.06C-1.8Mn-0.15Mo (DP)	55 pct	1	7.2×10^{16}	350
Ollat[1]	micro-alloyed DP1000 (see Table II)	55 pct	1	3×10^{15}	326

time and temperature. Under a number of simplifying assumptions and considering isothermal conditions, this equation can be written as follows :

$$F(T,t) = 1 - \exp(-(bt)^n) \quad [1]$$

where

$$b = b_0 \exp\left(-\frac{Q}{RT}\right) \quad [2]$$

This type of modeling is thus very simple and requires the determination of three parameters: n (the Avrami exponent), Q (the activation energy), and b_0 (a rate constant). These parameters can be easily obtained from the experimental recrystallization kinetics determined below the Ac_1 temperature (*i.e.,* before any austenite formation). Then, once the parameters have been determined, the recrystallization kinetics can be predicted under isothermal or non-isothermal conditions. This type of approach has been widely used in the literature[1,8–11] for different steel chemistries, as illustrated in Table I. In particular, it was used to build interaction maps between recrystallization and austenite formation during the heating stage of Dual-Phase steels by coupling the JMAK model for recrystallization with a JMAK model for austenite formation (case of Kulakov *et al.*[8] on a DP600 steel) or with experimental austenite formation kinetics (case of the work of Ollat *et al.*[1] on a DP1000 steel).

The main drawback of this type of approach is that it is unable to predict the influence of changes in chemical compositions and reduction ratios. As can be seen from the data of Table I, such changes lead to different values of the three parameters of the model but the link between the values of n, Q, and b_0 and the chemical composition or the reduction ratio is not obvious. This is why, Sinclair *et al.*[12] came back to the original JMAK formalism and proposed an extended recrystallization model in which the different parameters of the microstructure are linked to physical parameters. In particular, these authors were able to explain the slower recrystallization rates induced by the presence of Niobium in pure iron by taking into account the segregation of this alloying element within the interface.

In the above-mentioned context, the objective of the present study is to generalize the extended recrystallization model formalism developed by Sinclair *et al.*[12] to the different types of alloying elements present in the chemical composition of Dual-Phase steels by linking the predicted kinetics to the chemical composition and to the diffusion coefficients of the elements. This microstructurally based model for recrystallization (denoted MiReX) was first tested on ternary ferritic-pearlitic Fe-C-Mn alloys with various C and Mn contents and cold-rolled with three different reduction ratios, in order to adjust the parameters of the model relative to the Mn content and to the reduction ratio. The effect of other alloying elements (Si, Cr, and Mo) was also analyzed using recrystallization kinetics from the literature. Lastly, the model was tested on two industrial DP steels: a DP600 steel and the micro-alloyed DP1000 steel studied in the paper of Ollat *et al.*[1] In the latter case, the recrystallization model was coupled with a precipitation software (PreciSo) to take into account the effect of the micro-alloyed precipitates formed before or during recrystallization on the kinetics. Lastly, a discussion on the possible interaction between recrystallization and austenite formation during the annealing of cold-rolled DP steels was proposed.

II. MATERIALS AND PROCEDURES

A. *Material*

This study was carried out on four ternary Fe-C-Mn steels prepared in laboratory and on two industrial dual-phase steels. Their chemical composition is given in Table II. The chemical composition of the ternary steels was selected to be close to that of the industrial steels in terms of C and Mn contents. Moreover, the C and Mn contents of the ternary steels were chosen in order to be able to analyze clearly the effect of these two elements on the recrystallization. Concerning the industrial steels, they have almost the same Mn, Cr, and Si content but they differ mainly by their C content and by the presence of microalloying elements (Ti, Nb) in the case of the DP1000 steel. Additional initial microstructural information (pearlite fraction and initial ferrite grain size) was determined from optical observations of the microstructure after a Nital etching using ImageJ and is reported in Table II.

The Fe-C-Mn ingots were cast and hot forged to obtain bars with a 50 mm diameter and with a ferritic-pearlitic structure. The samples for the experimental study of the recrystallization were machined by

Table II. Chemical Composition and Microstructural Features of Ternary and Industrial Steels Investigated in This Study

Steel Grades	Chemical Composition (in Wt Pct)							Grain Size (μm)	Pearlite Fraction	Ac_1 (K)
	C	Mn	Cr	Si	Nb	Ti	N			
Ternary Steels	0.17	0.5	—	—	—	—	—	45	20	991
	0.17	1.7	—	—	—	—	—	30	28	978
	0.17	2.5	—	—	—	—	—	20	34	969
	0.08	1.7	—	—	—	—	—	50	15	978
DP 600	0.09	1.5	0.5	0.3	—	—	—	6	26	997
DP1000	0.17	1.7	0.4	0.3	0.03	0.03	0.006	6	36	993

Ac_1 values were calculated using Andrew's formula *et al.*[13]

wire-cut electroerosion and then, cold-rolled with a hand-operated rolling mill. Three different reductions ratios (25, 50, and 75 pct) were used to analyze the effect of this parameter on the recrystallization kinetics.

Concerning the two industrial steels, they have been hot-rolled in the austenitic phase, coiled around 873 K (600 °C), and slowly cooled to obtain a ferritic-pearlitic structure. The sheets were finally cold-rolled with a 55 pct reduction ratio to obtain sheets of 1.5 mm thick.

Annealing treatments on the DP600 steel and on the ternary steels were performed in salt baths. Samples (10 mm wide by 10 mm long) were treated at different temperatures for different times between 873 K (600 °C) and 923 K (650 °C) before being water-quenched in order to follow the recrystallization using hardness measurements.

Thermal treatments on the DP1000 steel were performed in a Gleeble 3500 thermo-mechanical simulator[14] heating by Joule effect and cooling through direct water projection on the specimens. Samples (10 mm wide by 100 mm long) were rapidly heated to the chosen temperature with a heating rate of 100 K/s and then, isothermally treated with a precise temperature control (± 3 K) thanks to the use of type-K thermocouples welded on the surface of the specimens. The annealing was interrupted by rapid water cooling after different treatment times in order to follow the microstructural evolutions with time at the considered annealing temperature. It has been checked that both heating techniques (*i.e.*, Gleeble and salt bath) lead to similar result on DP1000 steel.

B. *Determination of the Recrystallization Kinetics*

In order to determine the experimental recrystallization kinetics of the steels in the ferritic domain, Vickers hardness measurements were performed on the steels annealed for different times at the chosen recrystallization temperature(s) within the range 923 K to 973 K (600 °C to 700 °C), below Ac_1. For each treatment, about 15 measurements were performed at quarter thickness and with a 0.5 kg load. This led us to determine the recrystallized fraction (F_{rex}) which was calculated with the following relation:

$$F_{Rex} = \frac{H_0 - H(t)}{H_0 - H_F} \quad [3]$$

in which H_0, $H(t)$, and H_F correspond, respectively, to the initial hardness (after cold rolling), the hardness after a time t at temperature T, and the hardness of the fully recrystallized steel.

The uncertainties associated with the use of Eq. [3] were estimated at 10 pct and have been validated by comparing this method with optical observation. With regard to the interaction between precipitation and recrystallization, only the DP1000 can exhibit precipitation (cementite does not influence the hardness of the steel). Furthermore, for the DP1000, the precipitates can at most increase the hardness of 25 Hv.[15] This value represents a maximum error of 20 pct compared to the hardness difference observed due to recrystallization.

C. *Determination of the Austenite Formation Kinetics*

The austenite formation kinetics of the DP600 and DP1000 steels were experimentally determined using an optical dilatometer setup on a Gleeble machine. The optical system avoids any dilatometer stress on the sample. The classical lever rule was used to monitor the austenite fraction during continuous heating from room temperature to 1173 K (900 °C).

III. DESCRIPTION OF THE MICROSTRUCTURALLY BASED MODEL FOR RECRYSTALLIZATION (MIREX MODEL)

A. *Fundamental Equation*

As explained in the introduction, the objective of the model developed in this study is to be able to predict the influence of each alloying element (either in solution or precipitated) as well as that of the reduction ratio on recrystallization kinetics. The model is based on the work done by Sinclair *et al.*[12] relying on the JMAK formalism. In this approach, for a transformation involving nucleation and growth and considering that the nuclei of the new phase are randomly distributed, the real transformed fraction can be expressed as follows:

$$F_{Rex} = 1 - \exp(-F_{Ext}) \quad [4]$$

Table III. Values of the Key Parameters Used in the MiReX Model

Parameter	Symbol	Unit	Value Used
Average Recrystallized Grain Radius at Interface	R_{Int}	m	1×10^{-5}[12]
Avrami Exponent	n	-	1.3
Shear Modulus	μ	Pa	7.93×10^{10}
Burgers Vector in α-Fe	b	m	2.48×10^{-10}[12]
Interfacial Energy of Grain Boundaries in α-Fe	γ_{gb}	J m^2	0.38
Taylor Factor	M	—	3
Constant	α	—	0.25
Turnbull Factor	β	—	0.7[12]
α-Fe Molar Volume	V_m	$m^3 mol^{-1}$	7.09×10^{-6}[12]
Grain Boundary Thickness	δ	m	10^{-9}[12]
Gas Constant	R	J $mol^{-1} K^{-1}$	8.314
Coefficient Decribing the Transinterface Diffusivity	ϕ	—	15[12]
Pre-exponential Factor for Fe Diffusivity Along Grain Boundaries	D^0_{gb}	$m^2 s^{-1}$	1.5×10^{-4}[12]
Activation Energy for Fe Diffusity Along Grain Boundaries	Q_{gb}	kJ mol^{-1}	148[12]

where F_{Ext} is the extended transformed (here, recrystallized) volume fraction. It represents the transformed fraction if the nuclei grow through each other and overlap without interfering.

Assuming saturation of the nucleation sites, N_{Rex}, during transformation, the extended recrystallized volume fraction F_{Ext} can be written as follows for a non-homogeneous growth in the three directions of space:

$$F_{Ext} = N_{Rex}\left[\int_0^t \dot{R}dt\right]^n \quad [5]$$

where N_{Rex} corresponds to the density of nucleation sites available for recrystallization in the material, $\dot{R}$ accounts for the evolution of the recrystallized grain radius with time, and n is the Avrami exponent generally considered constant at different temperatures.

The growth rate of the nuclei, $\dot{R}$, is supposed to be proportional to the mobility of the recrystallization front (M) as well as to the energy available for the transformation of a deformed grain into a new recrystallized grain (G_{Rex}) and can be expressed by the following relation:

$$\dot{R} = MG_{Rex} \quad [6]$$

This leads to define the extended recrystallized volume fraction as follows:

$$F_{Ext} = N_{Rex}\left[\int_0^t M(X_{Mn}, X_{Cr}, \ldots, T)G_{Rex}dt\right]^n \quad [7]$$

where G_{Rex} is supposed to depend on the reduction ratio as well as on the presence of microalloying elements (which may precipitate before or during recrystallization) and M is likely to vary with the temperature as well as with the content of each type of substitutional element.

Here, one can note that the model can be used both for isothermal and non-isothermal treatments as it may take into account the variations of input parameters during recrystallization.

B. *Avrami Exponent n*

With regard to the Avrami exponent, it should be equal to 3 for isotropic growth of recrystallized ferrite grains. However, as the microstructures of the studied materials have been cold-rolled before annealing, this leads to an anisotropy during the growth of the grains. Consequently, this requires a reduction of the value of this parameter. Taking into account the experimental values determined in the literature for the Avrami coefficient by different authors[1,8–11] and recalled in Table I, the value of this parameter was fixed to 1.3 (Table III) for all compositions and it was supposed to be independent of the chemical composition, reduction ratio, and parameters of the thermal cycle.

C. *Nucleation Site Density N_{Rex}*

The nucleation site density, N_{Rex}, was evaluated by Sinclair *et al.*[12] from the measurement of recrystallized grain sizes in areas that have been freshly recrystallized. Their choice to study recrystallization with a temperature and niobium gradient within a unique sample allowed them to have all the steps of the recrystallization kinetics. So, they could observe the area for which recrystallization has just been completed. Then, they estimated to about 10μm the average grain radius at the interface (R_{Int}). So, it makes possible to calculate the density of nuclei available for recrystallization in the case of an inhomogeneous growth of dimension n using the following formula:

$$N_{Rex} = \left(\frac{1}{R_{Int}}\right)^n \quad [8]$$

Table IV. Link Between the Cold Rolling Reduction Ratios and the Dislocation Densities Within Steels

Reduction Ratio	Dislocation Density	Vickers Hardness
(*Pct*)	(m^{-3})	difference (kg mm^{-2})
25	5×10^{13}	37
50	2.4×10^{14}	80
75	5×10^{14}	116

Several phenomena could play a role on this value but for the sake of simplicity and universality of the model, this parameter will be considered, in the present work, as independent of the chemical composition, reduction ratio, and of the thermal cycle. Indeed, the effect of the N_{Rex} variation remains of a second order compared to the effect of the driving and pinning pressures controlling the growth rate.

D. *Driving Pressure for Recrystallization G_{Rex}*

The driving pressure available for recrystallization is related to the energy stored during cold rolling, $G_{rex,0}$, which can be expressed as follows:

$$G_{rex,0} = \frac{1}{2}\mu\rho b^2 \quad [9]$$

where ρ is the dislocation density, μ the shear modulus of α-Fe, and b the Bürgers vector in α-Fe. $G_{Rex,0}$ is expected to evolve with time due to the decrease in the dislocation density occurring during recovery. However, this evolution will be neglected in the present study, assuming that above 873 K (600 °C) the decrease in the quantity of dislocations is only due to recrystallization, which is the most energetically favorable phenomenon in this temperature range. In addition, the driving pressure due to the shape change (from elongated to spherical) between deformed and recrystallized grains is neglected.

In the case of micro-alloyed steels containing Nb and Ti, the driving pressure for recrystallization can be reduced by the Zener pinning effect due to the presence of complex carbides of TiNbC type and can then be written in the following general form[16,17]:

$$G_{\text{Rex}}(t) = G_{rex,0} - \frac{3}{2}\gamma_{\text{gb}}\frac{f_v}{R} \quad [10]$$

where γ_{gb} represents the interfacial energy of the grain boundaries, f_v the volume fraction of precipitates within the steel, and R their radius.

As highlighted by relation 9, the steel reduction ratio during cold rolling is expected to be a key parameter on recrystallization kinetics, as it is likely to modify the dislocation density in the material. In previous studies of the literature,[12] the dislocation density for cold-rolled steel sheets has been estimated from the hardness difference, ΔH, between the cold-rolled and recrystallized states of the material, assuming that the hardness difference is sensibly related to the difference in yield strength, $\Delta\sigma$, according to the following relation:

$$\Delta\sigma = \frac{\Delta H}{3} \quad [11]$$

and that

$$\Delta\sigma = M\alpha\mu b\sqrt{\rho} \quad [12]$$

where M is the Taylor factor and α is a constant. Their values are given in Table III.

Using this methodology on the ternary Fe-C-Mn steels investigated in this study after cold rolling with three different reduction ratios, the dislocation density was evaluated for these reduction ratios. Table IV gives the dislocation densities used in this work for three distinct reduction ratios. The following relationship allows us to estimate the density of dislocations within the ferritic-pearlitic microstructure for deformation ratios between 25 and 75 pct:

$$\rho = (5,6 \times 10^{10}\tau^2 + 3,4 \times 10^{12}\tau - 7 \times 10^{13})\text{m}^{-2} \quad [13]$$

where τ represents the cold rolling reduction ratio.

The model can be extended to different initial microstructures (*e.g.,* martensite, bainite) by adjusting some of the parameters (dislocation density, nucleation site density). It is worth mentioning that some authors decided for example to adjust the initial dislocation density successfully for a ferritic-martensitic microstructure.[18]

E. *Determination of the Interface Mobility Due to Segregation*

1. *Equation governing mobility*

The fundamental hypothesis driving the interface mobility is that it is slowed down by the segregation of substitutional elements to grain boundaries. This deceleration can be approximated with the slow part of Cahn's segregation model,[19] in the case where the energy available for transformation is low and below a critical value that has been validated by Sinclair *et al.*[12] This hypothesis enables, for low transformation energies, to suppose that the mobility is proportional to the interface mobility in pure iron (M_{pure}) and depends on the content of each type of alloying element according to relation 14:

$$M\left(T, X_{\text{Mn,Cr,Si,Mo,Nb,Ti}}\right) = \frac{M_{\text{pure}}}{1 + M_{\text{pure}}\sum_{i=1}^{n}\alpha_i X_i} \quad [14]$$

In relation 14, α_i is a slowdown coefficient reflecting the influence of the segregation of each type of

substitutional element within the interface on the interface mobility, X_i is the molar fraction of element i, and M_{pure} is the intrinsic grain boundary mobility in the case of pure iron. It is assumed to evolve with the temperature T according to relation 15:

$$M_{pure} = \beta \frac{V_m \delta}{b^2 RT} D^0_{gb} \exp\left(-\frac{Q_{gb}}{RT}\right) \quad [15]$$

where V_m is the ferrite molar volume, δ the width of the grain boundary, and R the universal gas constant. D^0_{gb} and Q_{gb} are, respectively, the pre-exponential factor and the activation energy of the intrinsic diffusion coefficient of Fe along the grain boundaries. Table III summarizes the values used in this work for all the model parameters.

With regard to the slowdown coefficient, α_i, of each alloying element, it is given by the following relationship:

$$\alpha_i = \frac{(RT)^2 \delta}{V_m E^i_b D^{Int}_i} \left(\sinh\left(\frac{E^i_b}{RT}\right) - \frac{E^i_b}{RT}\right) \quad [16]$$

It depends on the binding energy (E^i_b) of the considered element to grain boundaries and on its diffusion coefficient in iron $\left(D^{Int}_i = \phi D^0_i \exp\left(-\frac{Q_i}{RT}\right)\right)$ where $\phi = 15$[12] is a coefficient describing the real transinterface diffusivity based on the diffusion coefficients of the elements within the bulk.

Due to their major role on the recrystallization kinetics, the parameters (E^i_b and D^{Int}_i) involved in the calculation of the influence coefficient α_i of each element on the interface mobility have to be chosen very carefully. This is why, this particular point is discussed in the next section.

2. *Choice of the values of the binding energy and of the diffusion coefficient for each element*

The unknown parameters of the model are the diffusion coefficients of each element and their binding energy within the interface. These two parameters are difficult to measure and could be used as adjustable parameters. However, since our objective is to be able to provide a predictive model whatever the composition of the steels is, it has been chosen to use the values of these coefficients provided in the literature for each element when they are available.

As far as the values of D^0_i and Q_i are concerned, they have been fixed for all simulations. Table V summarizes the data used to calculate the diffusion coefficients throughout the simulations for Mn,[20] Cr,[21] Si,[22] Nb[21], and Mo.[21]

For the binding energies, the values of the substitutional elements with a strong interaction such as niobium[12] and molybdenum[23] or manganese[24] (which is the fundamental element of Dual-Phase steels) have been studied in the literature. These values were applied in the model. In the case of Cr and Si for which no binding energy was reported in the literature, it was chosen to apply the same reported value as for manganese and to check, a posteriori, that the chosen value is consistent or not with the experimental results.

Table V. Values of the Diffusion Coefficients and Binding Energies Used in This Work for Each Element

	Diffusion Coefficients		
Elements	Pre-exponential factor ($m^2.s^{-1}$)	Q (kJ/mol)	E_b (kJ/mol)
Mn	1.48×10^{-4}[20]	233 [20]	5 [24]
Cr	3.7×10^{-3}[21]	267 [21]	5
Si	1.97×10^{-4}[22]	218 [22]	5
Mo	1.48×10^{-2}[21]	282[21]	13.5[23]
Nb	1.5×10^{-1} [21]	299[21]	28.9[12]

Here, it has to pointed out that titanium, which enters in the chemical composition of the DP1000 steel of this study, was not considered in Table V because its diffusion coefficient and its binding energy in steel are not accurately known. This is why, the influence of this element will be neglected for the study of the DP1000 steel. This analysis is supported by the results of Bellavoine *et al.*[18] on steels containing Ti and/or Nb. They clearly highlight that the influence of this element on recrystallization is weaker than that of Nb.

At this stage, one can note that other combinations of diffusion coefficients and binding energies could be used. However, it is important to point out that this set of parameters coming from data of the literature was fixed throughout the rest of the present paper and it was no longer modified. Hence, the only input data to the model are the chemical composition and reduction ratio of the steel sheet and the parameters of the thermal cycle.

F. *Case of the Micro-alloyed Steels: Description of the Thermodynamic Model for Precipitation*

The prediction of the recrystallization kinetics of micro-alloyed steels containing Ti and Nb is more complex since the kinetics can be delayed both by a pinning effect of the grain boundaries by the complex (Ti,Nb)C carbides that may form before or during the recrystallization and/or by the segregation within the interfaces of the Ti and Nb atoms remaining in solid solution. It is therefore essential to be able to predict the precipitation kinetics of these carbides throughout the whole thermal cycle of these steels. In particular, the volume fraction (f_v) of the precipitates within the steel and their radius R are required as well as the solute fraction remaining in solid solution.

In this work, the Preciso software[25,26] was used to follow the evolution of the precipitation state of the (Ti,Nb)C carbides during heat treatments of the DP1000 steel of this study. It is based on the classical nucleation, growth, and coarsening theories, fully described by Wagner *et al.*[27] The precipitation state was characterized by the whole precipitate size distribution (Lagrange-like approach).

Thermodynamic calculations for a steel having the chemical composition of the DP1000 of the present study have shown that during hot rolling, precipitation is not able to reach the steady state predicted by Thermocalc.[28] However, during cooling, TiN precipitates can appear at high temperature in austenite, thus reducing slightly the Ti content in solid solution. Taking into account the slight decrease in the Ti content due to this precipitation, the TCFE8 database[29] gave a relatively constant composition of the (Ti,Nb)C carbides that can form during subsequent cooling at lower temperature: $(Ti_{0.36\pm0.05}, Nb_{0.64\pm0.05})C_{1\pm0.02}$ in austenite between 1473 K (1200 °C) and 973 K (700 °C) and $(Ti_{0.6\pm0.05}, Nb_{0.4\pm0.05})C_{1\pm0.02}$ in ferrite between 973 K (700 °C) and 573 K (300 °C). Thus, a simplified average composition was taken into account for each temperature domain. It was also assumed that the number of metallic (Ti and Nb) atoms was equal to the number of carbon atoms (no vacancy in precipitates), giving the following precipitate composition: $Ti_{0.36}Nb_{0.64}C$ in austenite and $Ti_{0.6}Nb_{0.4}C$ in ferrite. Then, using the evolution of austenite and ferrite composition with temperature at equilibrium, the solubility product was evaluated at each temperature with the following relations:

$$K_s^{\gamma} = (X_{Ti}^{eq,\gamma})^{0.36}(X_{Nb}^{eq,\gamma})^{0.64}(X_C^{eq,\gamma})^{1} \quad [17]$$

$$K_s^{\alpha} = (Xf_{Ti}^{eq,\alpha})^{0.6}(Xf_{Nb}^{eq,\alpha})^{0.4}(Xf_C^{eq,\alpha})^{1} \quad [18]$$

where $X_i^{eq,\alpha}$ and $X_i^{eq,\gamma}$ are the atomic fraction of element i in solution in ferrite and in austenite. Lastly, by linearly fitting the evolution of $log_{10}K_S$ with $\frac{1}{T}$, the following expression was taken for the solubility product of (Ti,Nb)C:

– in austenite:

$$\log_{10} K_s^{\gamma} = -\frac{9040\text{K}}{T} + 0.15 \quad [19]$$

– in ferrite:

$$\log_{10} K_s^{\alpha} = -\frac{5531\text{K}}{T} - 3.3 \quad [20]$$

Precipitate/matrix interface energy was taken equal to $0.35 \sim$ J m^{-2}, in order to be able to reproduce the experimental precipitation kinetics of the (Ti,Nb)C precipitates determined by Bellavoine *et al.*[18] under similar conditions and in accordance with Zurob's *et al.* values.[30]

IV. RESULTS

The aim of this section is to compare the predictions of the MiReX model for recrystallization with experimental recrystallization kinetics. This comparison is first performed on the Fe-C-Mn ternary alloys of this study in order to validate the effect of the reduction ratio and of the chemical composition (C and Mn content). Then, the effect of the presence of different alloying elements (Cr, Si, Mo) is presented and discussed using recrystallization kinetics extracted from the literature. Finally, the coupling of the recrystallization model with a software for predicting precipitation kinetics is performed to validate the model on an industrial micro-alloyed DP1000 steel.

A. *Modeling of the Recrystallization in Ternary Fe-C-X Systems*

1. *Case of the Fe-C-Mn system—Influence of the C and Mn content and of the reduction ratio*

The recrystallization model presented in Section III was first tested on the ternary steels of this study, in order to analyze separately the contribution of the (i) carbon content, (ii) manganese content, and (iii) reduction ratio on the recrystallization. For the validation of the model, the recrystallization kinetics of the cold-rolled ternary steels were modeled and experimentally determined for a recrystallization temperature of 898 K (625 °C).

Figures 1a) and 1b) show the effect of the carbon content and that of the manganese content on recrystallization. As can be seen in Figure 1a), the change in the carbon content of steel (from 0.08C to 0.17C) without modifying the manganese content (1.7 Mn) has no effect on the experimental recrystallization kinetics. This conclusion is consistent with the model which also predicts that the amount of carbon in steel is not likely to influence the recrystallization kinetics. By contrast, as clearly highlighted in Figure 1b) for steels with 0.17C, manganese significantly retards recrystallization, since the kinetics is regularly shifted towards longer annealing times as the manganese content is increased. Figure 1b) shows that this effect is well taken into account by the model, which tends to indicate that the parameters of the model chosen for manganese and given in Table V are correct.

Figure 2 highlights the effect of the reduction ratio on the recrystallization of the ternary 0.08C-1.7Mn steel at 898 K (625 °C). In the case of Dual-Phase steels, this parameter is generally adjusted in order to control their microstructure during the intercritical annealing. The reduction ratio influences mainly the stored energy during the deformation: increasing the reduction ratio increases the available energy for recrystallization and thus accelerates this phenomenon. It is therefore essential for the model to be able to predict the influence of this parameter. As can be seen in Figure 2, with the data of Table IV obtained from hardness experiments, the agreement between the experimental and modeled kinetics is quite satisfying.

2. *Influence of the addition of Mn, Cr, Si, Mo, and Nb*

The preceding results showed that manganese is expected to play a major role on the recrystallization of DP steels. This is mainly due to its rather high concentration (between 1.5 and 2 wt pct) compared to

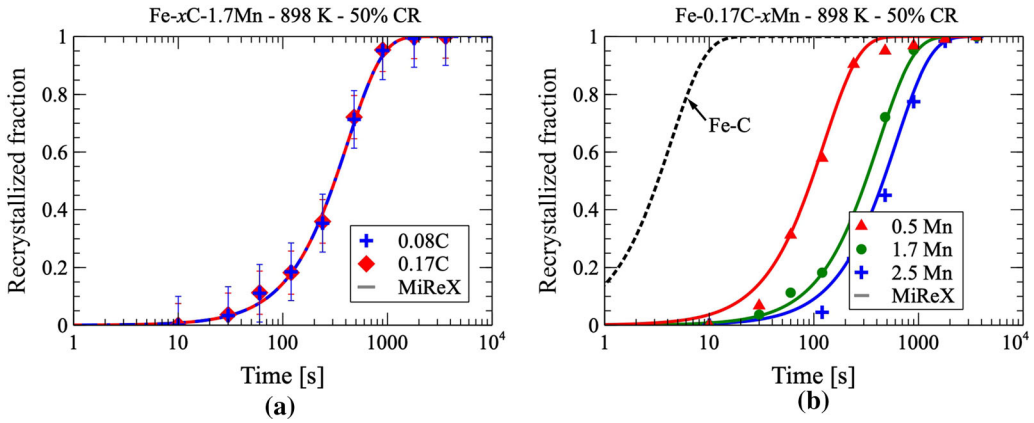

Fig. 1—Effect on the recrystallization kinetics at 898 K (625 °C) of ternary Fe-C-Mn steels cold-rolled with a 50 pct reduction ratio: (*a*) of the C content; (*b*) of the Mn content.

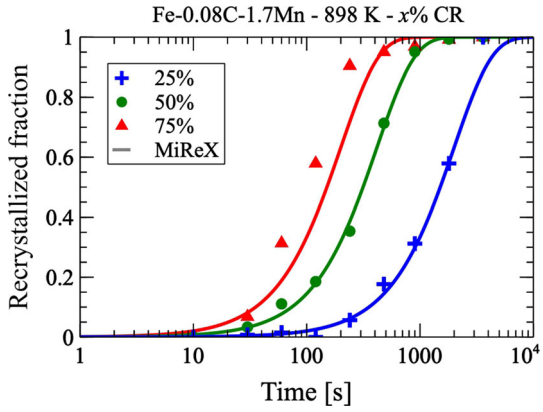

Fig. 2—Effect of the reduction ratio on the recrystallization kinetics at 898 K (625 °C) of the Fe-0.08C-1.7Mn steel.

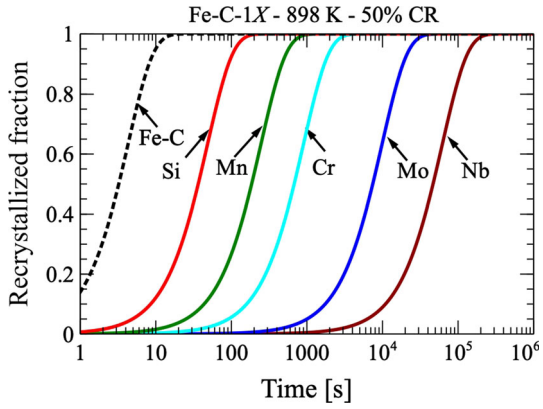

Fig. 3—Modeling of the effect of the addition of 1 wt pct alloying element on the recrystallization kinetics of a Fe-C-1*X* system with the data of Table V.

that of the other substitutional elements (such as Cr, Si, Mo, Nb) commonly present in the chemical composition of industrial DP steels.

However, in spite of their lower concentration in DP steels, these elements may influence the recrystallization. This is why, before testing the MiReX model on more complex systems combining several types of substitutional elements, it seems interesting to use this model to determine the relative influence of the typical alloying elements of DP steels on recrystallization. To this end, it was chosen to compare the effect of adding 1 wt pct of alloying element in a Fe-C-X system.

Figure 3 shows that among the three most widely used elements in DP steels (Mn, Si, Cr), silicon is expected to have less effect on the retardation of recrystallization than manganese or chromium. Concerning niobium and molybdenum, these elements have a very important ability to slow down recrystallization kinetics. This explains why they will often drive the overall kinetics although they are added in very small quantities to steels.

B. *Modeling of the Recrystallization in More Complex Systems: Analysis of the Influence of the Addition of Cr, Si, and Mo*

After having analyzed the recrystallization kinetics of ternary systems and calibrated the model for manganese and reduction ratio, the recrystallization model was then tested on more complex systems studied in the literature and reported in Table I, in order to determine notably the contribution of (i) silicon (added to avoid carbides), (ii) chromium (added to improve quenchability), and (iii) molybdenum (added to improve mechanical impact properties).

For model validation, experimental data were extracted from studies of literature on three systems[8,11]: (i) a Fe-0,18C-1,5Mn-1,7Si steel to study the effect of a high Si addition, (ii) a Fe-0,06C-1,8Mn-0,15Mo steel to analyze the effect of molybdenum, and (iii) a Fe-0,1C-1,8 Mn-0,35Cr-0.16Si steel to investigate the contribution of chromium. In each case, in order to highlight the contribution of each type of substitutional element of the chemical composition on the retardation of recrystallization, the recrystallization kinetics at 923 K (650 °C) was modeled for (i) the corresponding binary Fe-C system, (ii) the corresponding ternary Fe-C-Mn system, and (iii) the whole system including all the alloying elements of the chemical composition.

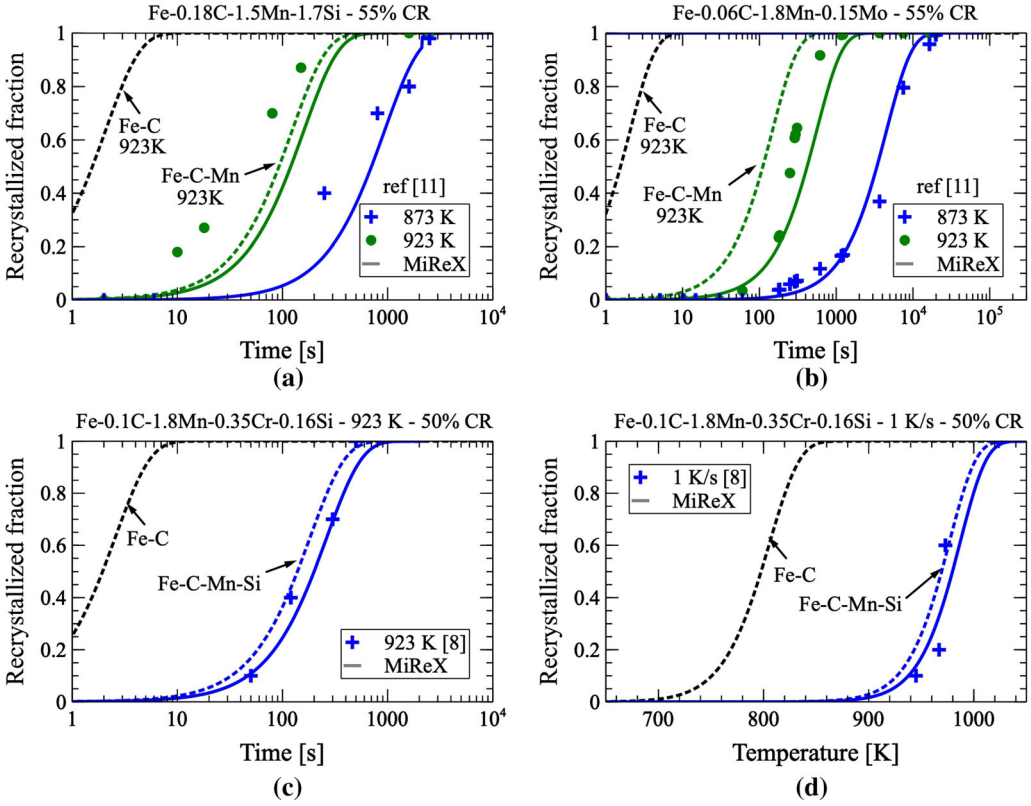

Fig. 4—Effect of (*a*) silicon; (*b*) molybdenum; (*c*) chromium on the isothermal recrystallization kinetics of cold-rolled Fe-C-Mn steels at 873 K and/or 923 K. (*d*) Non-isothermal recrystallization kinetics during continuous heating at 1 K/s of a cold-rolled Fe-0.1C-1.8Mn-0.35Cr steel.

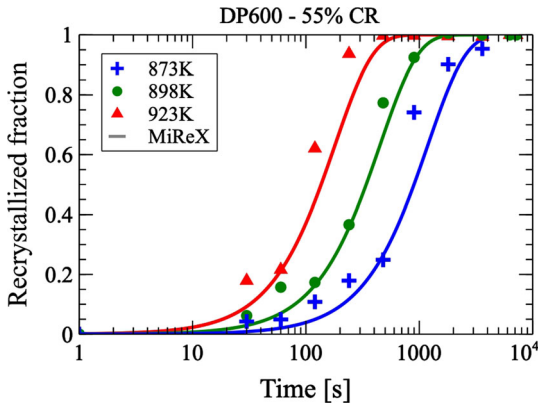

Fig. 5—Effect of the temperature on the recrystallization kinetics of the DP 600 steel cold-rolled with a 55 pct reduction ratio.

Figure 4(a) shows the effect of the silicon content on recrystallization. As can be seen in Figure 4(a), the experimental kinetics obtained by Huang[11] on a Fe-0.18C-1.5Mn-1.7Si steel are well predicted by the model. However, it is interesting to compare the simulations carried out on a Fe-C-1.5 Mn steel with 1.7 Si and without Si: they highlight that this element has a negligible impact on recrystallization, when it is added in a steel containing already a high manganese content.

Figure 4(b) shows the effect of the molybdenum content on the recrystallization kinetics of a Fe-0.17C-1.8 Mn-0.15Mo steel[11] at two temperatures. The slowdown of the experimental kinetics due to molybdenum segregation is well predicted by the model. Furthermore, the simulations on a Fe-C-1.8Mn steel with or without molybdenum show that the addition of this element, even in small quantities, has a much greater impact on the retardation of the recrystallization than a high addition of silicon.

Lastly, Figures 4(c) and (d) show the effect of the chromium content on the isothermal and non-isothermal recrystallization kinetics of a Fe-0.1C-1.8Mn-0.3Cr steel[8] assuming that no precipitation of chromium carbide occurs during the treatment. Unlike silicon, the chromium content has a non-negligible impact on recrystallization despite its low content in the alloy. Furthermore, Figure 4(d) shows that the model is likely to predict rather well recrystallization during continuous heating at 1 K/s. At first sight, it seems that it can be applied a priori to complex thermal cycles including a heating stage followed by a holding at the considered annealing temperature.

Table VI. Definition of the JMAK Parameters of the DP600 Steel

Grades	n	Q (kJ/mol)	b_0 (s^{-1})
DP600	1.3	355	9×10^{17}

C. *Modeling of the Recrystallization of Industrial DP Steels*

1. *Case of the DP600 steel*

In order to test the validity of the model on an industrial steel without microyalloying element, the recrystallization kinetics of the DP600 steel of this study was obtained experimentally at three temperatures and modeled. The influence of each element of its composition having been studied before, it is clear that the two main elements responsible for the slowdown of the kinetics compared to pure iron are manganese and chromium. Figure 5 shows the very good experimental agreement obtained when the MiReX model is used on the DP600 steel of this study at the three investigated temperatures.

Here, it has to be noted that the modeling of the recrystallization kinetics of the DP600 steel can also be performed with the JMAK model recalled in the introduction of this paper (Eq. [1]). Table VI gives the three parameters (n, b_0 and Q) of the JMAK model of the DP600 steel determined from the experimental kinetics of Figure 5. The activation energy is equal to 355 kJ/mol. It is much higher than that for iron self-diffusion in ferrite (250 kJ/mol) as it is an apparent activation energy.

2. *Case of the micro-alloyed DP 1000 steel*

For the study of the recrystallization of the DP1000 steel, it was first necessary to determine the degree of precipitation of Ti and Nb in the form of (Ti,Nb)C carbides at the end of the processing of the steel sheets (before the annealing step). This precipitation may occur either in austenite (during reheating of the slabs at 1523 K (1250 °C) and/or hot rolling during cooling) or in ferrite (during coiling at 873 K (600 °C) followed by air cooling to ambient temperature). Using the Preciso software and the methodology presented in Section III–E, the Time-Temperature-Transformation (TTT) diagrams of the DP1000 steel could be built. Figure 6(a) concerns the precipitation of the $Ti_{0.36}Nb_{0.64}C$ carbide in austenite (above Ac_1), while Figure 6(b) is relative to the formation of the $Ti_{0.6}Nb_{0.4}C$ carbide in ferrite (below Ac3). As can be seen in Figure 6, precipitation is expected to be much more rapid in ferrite than in austenite (notably between 850K and Ac3).

In addition, the TTT diagrams present the limiting grain diameter (D_l) reachable in the presence of the precipitation within the steel. This diameter was calculated, for each state, using the modified Zener equation[28]:

$$D_l = \frac{2R}{3f_v} \qquad [21]$$

where R and f_v are the radius and volume fraction of the precipitates.

Figure 6 shows that over short periods of time at a given temperature, no precipitation is expected. Then, when precipitation occurs, the limiting grain diameter decreases due to pinning pressure before increasing due to precipitate coarsening.

Taking into account the real industrial cycle of the studied steel and the TTT diagrams of Figure 6, it was possible to conclude that almost no precipitation occurred during the processing of the steel (hot rolling, coiling, and air cooling), suggesting that all the microalloying elements should be in solid solution before the annealing step.

In Figure 7(a), the MiReX model was thus tested at three annealing temperatures under two different conditions: (i) assuming that all the niobium atoms remain in solid solution during recrystallization and (ii) considering the precipitation of TiNbC particles during the annealing as predicted by PreciSo. As can be seen in Figure 7(a), the MiReX model is likely to reproduce the experimental isothermal recrystallization kinetics of the DP1000 steel with the two considered conditions. This can be explained by the fact that precipitation starts at a relatively late stage of recrystallization in all cases, so that the kinetics are not notably affected by this phenomenon. Nevertheless, a stronger interaction could be observed for lower cold rolling reduction ratios leading to slower recrystallization rates.

This is why, in order to compare the relative effect on the recrystallization kinetics of the pinning pressure exerted by the precipitates and of the solute Ti and Nb atoms, the DP1000 was pre-treated for 20 min at 973 K (700 °C) so that all the Ti and Nb leave the solid

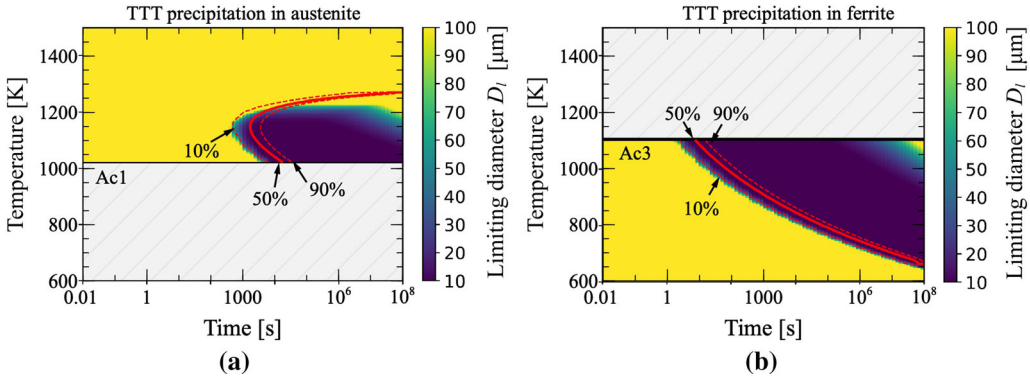

Fig. 6—TTT diagram for the precipitation of the (Ti,Nb)C carbides and limit grain size obtained by the Zener equation: (*a*) in austenite and (*b*) in ferrite.

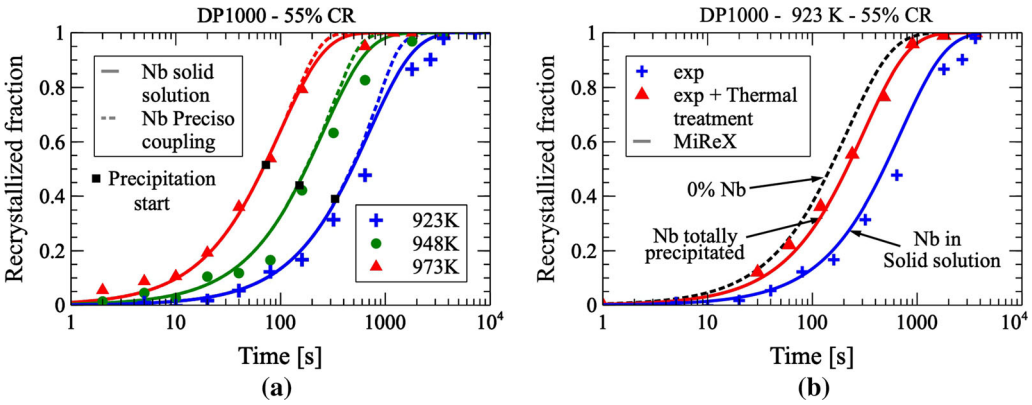

Fig. 7—Effect of (*a*) the temperature and (*b*) the precipitation state of Nb on the recrystallization kinetics of the DP 1000 steel cold-rolled with a 55 pct reduction ratio.

solution (as predicted by the TTT diagram of Figure 6(b)). It was then cold-rolled with a 55 pct reduction ratio before being annealed at 923 K (650 °C).

Figure 7(b) clearly shows the acceleration of the recrystallization kinetics when precipitates have formed before annealing, suggesting that their effect on the slowdown of recrystallization is less pronounced than that due to the segregation of the microalloying elements within the interface. This observation is in good agreement with the conclusions of Bellavoine *et al.*[18] and is well taken into account by the recrystallization model of this study when the effect of the precipitates is considered. It was therefore possible, during this study, to simulate the precipitation kinetics of (Ti,Nb)C carbides and to combine it with the recrystallization model in order to be able to reproduce the recrystallization kinetics of the Micro-alloyed DP1000 steel of this study. Here, one can note that the MiReX model could be extended to the study of the effect of other types of precipitates on the recrystallization.

V. DISCUSSION: INTERACTION BETWEEN RECRYSTALLIZATION AND AUSTENITE FORMATION

A. *Consequence of the Interaction on the Microstructure and on the Austenite Formation Kinetics*

As mentioned in the introduction of this paper, an interaction between recrystallization and austenite formation is likely to occur during the annealing of Dual-Phase steels, notably during the heating stage to the annealing temperature. This interaction has already been extensively studied in literature[1,8,9,11] and leads to two types of interactions called "weak" and "strong" by Chbihi *et al.*[31] The "weak" interaction corresponds to the case where the recrystallization is mostly completed at the austenite start temperature. By contrast, in the case of a "strong" interaction, recrystallization and austenite formation are assumed to occur simultaneously. This will affect (i) the recrystallization kinetics and (ii) the nucleation and growth of austenite. From an experimental point of view, this "strong" interaction can be observed (i) at high heating rate as the recrystallization domain is shifted to higher temperatures and/or (ii) with the presence of alloying elements (such as Mn,Cr,Mo,Ti,Nb) likely to segregate within the grain boundaries or to form precipitates.

A "strong" interaction results in a significant change in the final microstructure of Dual-Phase steels. Li *et al.*[9] described in detail the microstructures obtained for various heating rates. In the case of a weak interaction, austenite nucleation takes place at the ferrite-pearlite interfaces and recrystallized grain boundaries, leading to a rather homogeneous microstructure. In contrast, in the case of a "strong" interaction due to the use of a high heating rate (> 20 °C), a coarse, banded, and heterogeneous microstructure is obtained. Different explanations are given in the literature: (i) moving recrystallizing ferrite boundaries are not favorable sites for austenite nucleation; (ii) deformed ferrite grains are high-energy nucleation sites, so that the carbides near these grains are preferential nucleation sites; (iii) deformed ferrite grains may promote long-range carbon diffusion.

As already mentioned, the degree of interaction between recrystallization and austenite formation may affect the final microstructure and thus, the final mechanical properties. However, it is also likely to modify notably the austenite formation kinetics during heating. This is illustrated in Figure 8 which shows the kinetics obtained by dilatometry for the two industrial DP steels investigated in this study for a heating of 30 K/s starting from a cold-rolled state and from a recrystallized state. The austenite formation kinetics of the cold-rolled DP600 steel exhibits a slight acceleration at the beginning of the transformation compared to the recrystallized steel. This could be explained by the fact that the recrystallization phenomenon is not complete at Ac_1 for the considered heating rates. On the other hand, the austenite formation kinetics of the cold-rolled DP1000 steel presents a very strong acceleration throughout the transformation compared to the kinetics of the recrystallized steel, which could be due to a near-zero fraction of recrystallized ferrite at the start of the phase transformation.

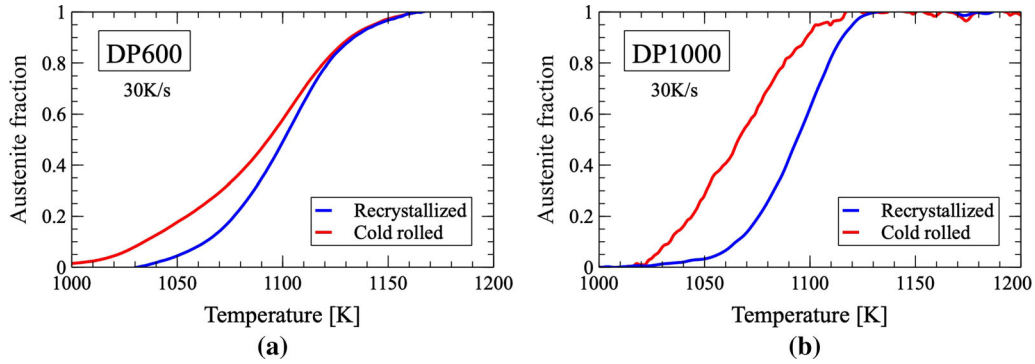

Fig. 8—Austenite formation kinetics during continuous heating at 30 K/s starting from a recrystallized and cold-rolled steel: (*a*) DP 600 steel: (*b*) DP 1000 steel.

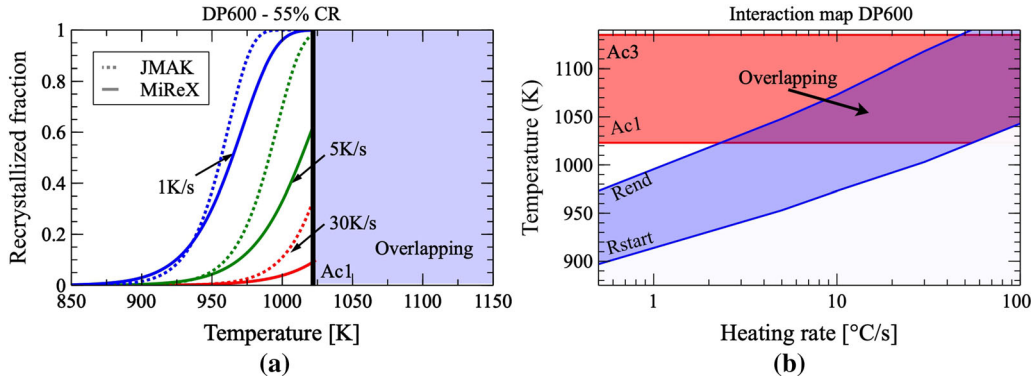

Fig. 9—(*a*) Modeled recrystallized fractions of the DP600 steel during continuous heating with three different heating rates using the simple JMAK formalism and the MiReX model; (*b*) Interaction map of the DP 600 steel.

The preceding considerations highlight the necessity to be able to model the recrystallization during continuous heating of the steel up to its annealing temperature in order to know the temperature domain for recrystallization and to predict whether an interaction with austenite formation will occur or not. The aim of the next section is thus to discuss about the modeling of recrystallization under non-isothermal treatments.

B. *Modeling of Recrystallization During Continuous Heating: Application to the Industrial Steels*

The modeling of the recrystallization under non-isothermal conditions can be easily performed from the simple JMAK formalism recalled in the introduction of this paper (Eq. [1]). After having determined the three parameters (n, b_0 and Q) of this equation using isothermal experiments performed below Ac_1, the differential form of the JMAK law can be used to predict the recrystallization during continuous heating:

$$\frac{dF(T,t)}{dt} = n \cdot (1-F) \cdot k(-\ln(1-F))^{\frac{n-1}{n}} \qquad [22]$$

This type of approach has already been used with success in literature by different authors[1,8,9,11] and it was partly validated thanks to a comparison of the modeled kinetics with experimental kinetics (determined as in the present study). However, one can note that the comparisons were always performed in the case where the heating rate did not exceed 10 K/s. Namely, in these conditions, the recrystallization domain is at relatively low temperature (mostly, below Ac_1) and thus, relatively close to the domain of the isothermal experiments which were used to determine the parameters of the model.

The MiReX model developed in this study can also be used under non-isothermal conditions. This was already done in the case of Figure 4(d) which corresponds to a continuous heating at 1 K/s. In this case, the model describes well the recrystallization and it gives similar results to those of the JMAK model based on Eq. [21] used by Reference 8.

JMAK model remains today one of the most used approach to study recrystallization kinetics due to its simplicity of application. In this context, it seems interesting to compare the modeling of recrystallization during continuous heating using (i) the JMAK approach based on Eq. [21] and (ii) the MiReX model. This comparison was performed in the case of the DP600 steel of this study for which the parameters (n, b_0 and Q) of the JMAK model are given in Table VI.

Figure 9(a) shows the comparison of the two types of recrystallization modeling during continuous heating with different heating rates used industrially from 1 to 30 K/s. Note that above Ac_1, autenite formation may

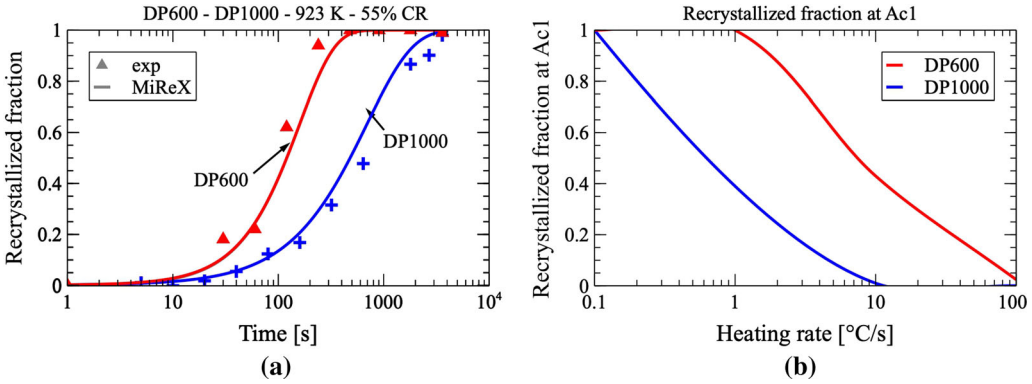

Fig. 10—(*a*) Experimental and modeled recrystallized fractions of the DP600 and DP1000 steels as a function of time at 923 K (No results are shown for temperatures above Ac_1 since phase transformation may strongly affect the ReX kinetics in the overlapping domain[32]). (*b*) Predicted recrystallized fractions at Ac_1 for the two steels with the MiReX model.

modify the recrystallization kinetics as highlighted by some authors.[10,31,32] Therefore, no results are shown above Ac_1 in figure 10. First of all, we can note a very good agreement between the two types of modeling for kinetics at 1 K/s as already mentioned in the case of Figure 4(d). For higher heating rates, the two types of modeling are in relatively good agreement as long as the temperature is below the Ac_1 temperature (around 1020 K). This is consistent with the fact that the models were calibrated in this temperature range and gave similar results in this temperature domain under isothermal conditions.

From the kinetics of Figure 9(a), the temperatures at which the recrystallization kinetics starts and ends (calculated for a recrystallized fraction of 5 and 95 pct) could be determined with the MiReX model for different heating rates (Figure 9(b)). The austenite start and austenite finish temperatures determined on previously recrystallized steel, by optical dilatometry, were also plotted leading to the interaction map of Figure 9(b) for the DP600 steel of this study. Interaction can only be observed for heating rates higher than 3 K/s. This is consistent with the results of Kulakov *et al.*[8] based on the simple JMAK Eq. [1]. Here, it is also important to point out the fact that the interaction domain of the micro-alloyed DP1000 steel determined by Ollat *et al.*[1] starts at lower heating rates. This is due to the fact that the microalloying elements (Ti and Nb) of the DP1000 steel significantly delay the recystallization kinetics, compared to the case of the DP600 steel, due to the segregation of these elements within the interface and/or by the formation of (Ti,Nb)C precipitates (Figure 10(a)). The consequence is that the recrystallization domain of the DP1000 steel is obtained at higher temperatures, thus decreasing the value of the minimum heating rate for which interaction starts to be detected.

To complete this work, the recrystallized fractions at the austenite start temperature predicted with the MiReX model were plotted as a function of the heating rate in Figure 10(b) for the DP600 and DP1000 steels of this study. At the lowest heating rates, no interaction is expected in the DP600 steel, while it can be important in the DP1000 steel. By contrast, above 10 K/s, a strong interaction is possible in the two steels as illustrated in Figure 8.

As a conclusion, these results highlight the importance of paying attention to industrial trends that tend towards the increasingly important addition of substitutional elements for the development of new grades and to the use of furnaces with higher heating rates (until 100 K/s). It is therefore essential to have a tool for predicting recrystallization kinetics as a function of chemical composition, thermal cycle, and reduction ratio to optimize chemical compositions and thermal paths.

VI. CONCLUSION

1. The modeling of the recrystallization kinetics of cold-rolled ferritic-pearlitic DP steels was performed using a microstructurally-based recrystallization model (denoted MiReX model) and likely to take into account the reduction ratio of the steel sheet, the pinning effect of the precipitates that may form before or during recrystallization, and the solute drag of substitutional elements (Mn, Si, Cr, Mo, Nb) within the interfaces. In this model, the effect of each type alloying element segregated within the interfaces on the retardation of the recrystallization kinetics was taken into account thanks to a slowdown coefficient depending on the diffusion coefficient of the element and its affinity to be segregated at grain boundaries. The data (diffusion coefficient, binding energy to grain boundaries) of each element were extracted from the literature. The kinetics predicted by the MiReX model were performed without any adjustable parameters and compared to a wide range of experimental kinetics.
2. A validation of the model was first conducted on ternary Fe-Mn-C alloys with various C and Mn contents and cold-rolled with different reduction ratios, in order to confirm the influence of the chemical composition (notably, of the Mn content)

and reduction ratio on recrystallization kinetics. It was observed that Mn due to its rather high concentration in DP steels plays a major role on the recrystallization kinetics which is significantly delayed compared to that of binary Fe-C steels.

3. The model was then confronted with experimental results from the literature on more complex systems of Fe-C-Mn-X type, representative of the chemical composition of DP or TRIP steels, notably to validate the influence of the addition of Si, Mo and Cr. Contrary to silicon, molybdenum may have a strong influence on recrystallization due to its low diffusion coefficient and its high binding energy to grain boundaries. A rather good agreement between the MiReX model and experiment was noted in a wide domain of chemical composition of AHSS and UHSS as well as standard cold rolling reduction ratios without fitting parameters.
3. In the case of the micro-alloyed DP1000 steel, a coupling with a precipitation modeling sofware was used to include the effect of the (Ti,Nb)C precipitates. It was highlighted that Ti and Nb have a crucial role in kinetics both in solid solution and as precipitates due to their pinning effect on the grain boundaries. The integration of precipitates into the MiReX model made it possible to reproduce the interaction of precipitation and recrystallization for micro-alloyed steels.
4. Lastly, the MiReX model was used to predict recrystallization during continuous heating and to analyze the possibility of interaction of this phenomenon with austenite formation. For DP600 steels, this type of interaction is expected for heating rates higher than 3 K/s and it leads to an acceleration of the austenite formation kinetics.

REFERENCES

1. M. Ollat, V. Massardier, D. Fabregue, F. Keovilay, E. Buscarlet, and M. Perez: *Metall. Mater. Trans. A*, 2017, vol. 48, pp. 4486–99.
2. B. Zhu and M. Militzer: *Model. Simul. Mater. Sci.*, 2012, vol. 20, pp. 1–17.
3. B. Scholtes, R. Boulais-sinou, A. Settefrati, D. Pino, I. Poitrault, A. Montouchet, N. Bozzolo, and M. Bernacki: *Comput. Mater. Sci.*, 2016, vol. 122, pp. 57–71.
4. R. Loge, M. Bernacki, H. Resk, L. Delannay, H. Digonnet, Y. Chastel, and T. Coupez: *Philos. Mag.*, 2008, vol. 88, pp. 3691–3712.
5. M. Bernacki, H. Resk, T. Coupez, and R.E. Logé: *Model. Simul. Mater. Sci.*, 2009, vol. 17, p. 64006.
6. C. Zheng and D. Raabe: *Acta Mater.*, 2013, vol. 61, pp. 5504–17.
7. M.S. Salehi and S. Serajzadeh: *Comput. Mater. Sci.*, 2012, vol. 53, pp. 145–52.
8. M. Kulakov, W.J. Poole, and M. Militzer: *Metall. Mater. Trans. A*, 2013, vol. 44A, pp. 3564–76.
9. P. Li, J. Li, Q. Meng, W. Hu, and D. Xu: *J. Alloys Compd.*, 2013, vol. 578, pp. 320–27.
10. D.Z. Yang, E.L. Brown, D.K. Matlock, and G. Krauss: *Metall. Mater. Trans. A*, 1985, vol. 16, pp. 1385–92.
11. J. Huang, W.J. Poole, and M. Militzer: *Metall. Mater. Trans. A*, 2004, vol. 35, pp. 3363–75.
12. C. Sinclair, C. Hutchinson, and Y. Bréchet: *Metall. Mater. Trans. A*, 2007, vol. 38, pp. 821–30.
13. K. Andrews: J. Iron Steel Inst., 1965, pp. 721–727.
14. Gleeble: Thermomechanical simulator 3500. https://www.gleeble.com/products/gleeble-3500.html, 2019.
15. R. Soto, W. Saikaly, X. Bano, C. Issartel, G. Rigaut, and A. Charai: *Acta Mater.*, 1999, vol. 47, pp. 3475–81.
16. P.R. Rios, G.S. da Fonseca: Grain Boundary Pinning by Particles, in: *Materials Science Forum*, Trans Tech Publications Ltd, 2010, vol. 638, pp. 3907–3912.
17. C.S. Smith: *Trans. Metall.*, 1948, vol. 175, pp. 15–51.
18. M. Bellavoine, M. Dumont, J. Drillet, V. Hébert, and P. Maugis: *Metall. Mater. Trans. A*, 2018, vol. 49, pp. 2865–75.
19. A.T. Wicaksono, A Note on the Cahn Solute Drag Model, 2015.
20. V. Irmer and M. Feller-Kniepmeier: *J. Phys. Chem. Solids*, 1972, vol. 33, pp. 2141–48.
21. N. Oono, H. Nitta, and Y. Iijima: *Mater. Trans.*, 2003, vol. 44, pp. 2078–83.
22. Thermo-Calc Software, MOBFE 3 Steels/Fe-Alloys Mobility Database 3, 2017.
23. HS. Zurob, D. Panahi, C.R. Hutchinson, Y. Brechet, and G.R. Purdy: *Metall. Mater. Trans. A*, 2012, vol. 44A, pp. 3456–71.
24. F. Danoix, X. Sauvage, D. Huin, L. Germain, and M. Gouné: *Scr. Mater.*, 2016, vol. 121, pp. 61–65.
25. M. Perez, M. Dumont, and D. Acevedo-Reyes: *Acta Mater.*, 2009, vol. 57, p. 1318.
26. M. Perez, M. Dumont, and D. Acevedo-Reyes: *Acta Mater.*, 2008, vol. 56, pp. 2119–2132.
27. R. Wagner, R. Kampmann, and P.W. Voorhees: *Phase Trans. Mater.*, 2005, vol. 5, pp. 309–407.
28. A. Graux, S. Cazottes, D. De Castro, D. San Martín, C. Capdevila, J.M. Cabrera, S. Molas, S. Schreiber, D. Mirković, F. Danoix, M. Bugnet, D. Fabrègue, M. Perez, Materiala, 2019, vol. 5, p. 100233.
29. Thermo-Calc Software, TCFE 8 Steels/Fe-alloys database version 8, 2017.
30. H.S. Zurob, C.R. Hutchinson, Y. Brechet, and G. Purdy: *Acta Mater.*, 2002, vol. 50, pp. 3077–94.
31. A. Chbihi, D. Barbier, L. Germain, A. Hazotte, and M. Gouné: *J. Mater. Sci.*, 2014, vol. 49, pp. 3608–21.
32. D. Barbier, L. Germain, A. Hazotte, M. Goune, and A. Chbihi: *J. Mater. Sci.*, 2015, vol. 50, pp. 374–81.

Publisher's Note Springer Nature remains neutral with regard to jurisdictional claims in published maps and institutional affiliations.